Mini Review

JOURNAL OF THE CHINESE CHEMICAL SOCIETY

Transitions between Electron Transporting Mechanisms in Molecular Junctions and Transistors

Chun-Ting Kuo, Li-Chen Su and Chun-hsien Chen*

Department of Chemistry and Center for Emerging Material and Advanced Devices, National Taiwan University, Taipei 10617, Taiwan

(Received: Oct. 1, 2013; Accepted: Nov. 20, 2013; Published Online: Dec. 9, 2013; DOI: 10.1002/jccs.201300504)

On the extraordinary journey cruising into the interdisciplinary field of molecular electronics by experimentalists, many of the proposed mechanisms for electron transporting across molecular junctions have been witnessed, such as hopping, direct tunneling, thermionic emission, and field emission. For a newcomer to this research field, the terms of the mechanisms can be confusing. This mini-review is intended to provide a very elementary introduction to the basics of the mechanisms with the help of selected literature examples to make the concept less abstract. In addition to the definition of terminologies used in molecular electronics, the correlation of experimental conditions with the pathways of electron transport is emphasized.

Keywords: Molecular electronics; Electron transport mechanisms; Molecular junction; Single-molecule conductance.

Chun-hsien Chen *obtained his BS degree in 1986 from National Sun Yat-sen University and PhD degree in 1993 from the University of Illinois at Urbana-Champaign. After spending two years as a postdoctoral research associate at The University of North Carolina at Chapel Hill, he joined the Department of Chemistry at National Sun Yat-sen University. He moved to National Tsing Hua University in 2000 and to National Taiwan University in 2006. His research interests involve electrochemistry and scanning probe microscopy on phenomena at the solid-liquid interface. He is a distinguished professor of NTU, a recipient of the Chinese Chemical Society Young Chemist Award (2001), NTHU Young Investigator Award (2002), Outstanding Research Award from NSC (National Science Council, 2008), and Y. Z. Hsu Scientific Paper Award (2009).*

Chun-Ting Kuo *received his BS (2004) and MS (2006) degrees from National Tsing Hua University, and PhD degree in 2010 from National Taiwan University. He is currently a postdoctoral research associate at the University of Washington (Seattle). His research interests involve high performance liquid chromatography, the synthesis and size control of gold nanoparticles, employing gold nanoparticles as sensing probes, and I-V characteristics of single-molecule transistors. He is awarded the Postdoctoral Research Abroad Program by National Science Council (2013).*

Li-Chen Su *received her BS degree in 2005 from Tunghai University. Her MS and PhD degrees were awarded in 2007 and 2012 from National Central University. She is currently a postdoctoral research associate at National Taiwan University focusing on the electric behaviors at single-molecule junctions. Her research interests involve the development of ultra-sensitive biosensors based on surface plasmon resonance and metal-enhanced fluorescence.*

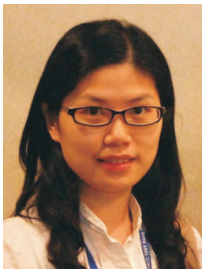

Special Issue for the 60th Anniversary of Journal of the Chinese Chemical Society

* Corresponding author. Tel: +886 2 3366 4191; Fax: +886 2 2363 6359; Email: chhchen@ntu.edu.tw

Molecular electronics, first proposed by Aviram and Ratner in 1974,[1] describes how the charge transport between electrodes is mediated by the energy levels of a single molecule or molecular thin films upon being subjected to external stimuli such as light, electric, and magnetic fields.[2,3] Configurations of electrode-molecule-electrode junctions have been devised to gain the fundamental understanding of the electric behaviors down to the single-molecule level.[2] The progress over the past decade has made the measurement schemes more attainable and the inter-laboratorial variations in the reported values of single-molecule conductance become less significant.[2] Concomitantly, mechanisms of electron transport projected in the theoretical work are demonstrated by the experimental advancement.[4] However, the terminology used for the mechanisms is rather abstruse and difficult to understand, particularly for those who just come across this field. Therefore, this mini-review attempts to elucidate the terms using experimental examples in which the conditions and results might provide a more approachable aspect to comprehend the mechanisms. In the following, the experimental designs and electron transporting mechanisms will be briefly introduced. Transition between mechanisms will then be discussed with literature examples using two- and three-terminal devices.

Molecular junctions

An apparent challenge for quantitative studies of molecular conductance is the incorporation of the nanometer-sized molecules into the electrical circuitry of the macroscopic source-measurement unit. To connect the probing electrodes to the molecular termini, an intuitive configuration is the MMM (metal-molecule-metal) format. The experimental fabrication of molecular junctions is now reasonably accessible and the results are more reproducible than those in the early days. Hence, it becomes practical to explore examples of MMM characteristics mimicking functional devices such as electrical switches, rectifiers, optoelectronics, thermoelectronics, and spintronics.[3] To facilitate the description of the charge transport mechanisms, Figure 1 illustrates conceptually the measurement schemes employed by literature reports cited in this mini-review.

Mechanically controllable break junction (MCBJ, Figure 1a) is a two-electrode platform, invented for a brittle superconducting film in 1985 by Moreland and Ekin[5] and first introduced for the measurements of single-molecule conductance in 1997 by Reed and co-workers.[6] The junctions to host molecules were made of a grooved gold wire initially or more recently lithographically developed structures.[7] Underneath the structure, there is a pushing rod. The movement of the rod against the counter supports (small blue dots at both sides) expands or reduces the junction in which, to certain points, the pre-deposited molecules are disrupted from one of the electrodes or the two electrodes are shorted together. By monitoring the current at a fixed bias voltage, conductance-distance traces, G(s), are acquired repeatedly by running the push-pull routine of the rod. The strength of contemporary MCBJ is the precise and stable control over the junction spacing.[8] With the incorporation of an aluminum gate electrode underneath the gold electrodes, the MCBJ becomes a three-terminal device.[7]

Molecular junctions created by SPMs (scanning probe microscopes) are relatively popular in this research field. For example, MMM junctions can be furnished with molecular monolayers sandwiched between the substrate and a conductive AFM tip (atomic force microscope) with[9-11] (Figure 1b) or without[12-15] (not shown) nanoparticles to limit the number of molecules in the gap.

Figure 1c illustrates the method of STM BJ (scanning tunneling microscopic break junction), first demonstrated using gold electrodes in 2003 by Tao and co-workers.[16] The experimental settings drive the STM tip into contact, getting fused with the substrate, and subsequently retracted. The tip pulls out a string of gold atoms which, upon being ruptured, snap back to the tip and substrate. Because of the sudden increase in the tip-substrate distance, the snap-back motion shortens the duration when tunneling current exhibits significant contribution and hence renders G(s) traces a distinct sharp drop.[17-19] The experiments are conducted in solution containing molecules of interest, which might bridge the gap and develop a MMM junction. The protocols are applicable to conductive AFM and yield the

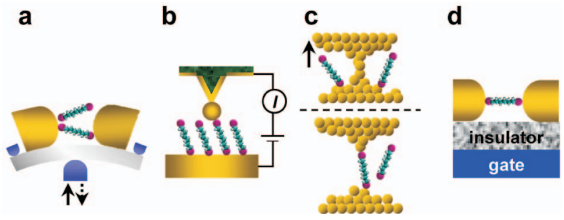

Fig. 1. Schematics for methods to furnish the molecular junctions. (a) MCBJ (mechanically controllable break junction); (b) cAFM (conductive atomic force microscope); (c) SPM BJ (scanning probe microscope break junction); (d) SMT (single-molecule transistor). The pictures are illustrative and not drawn to scale.

method of AFM BJ which offers simultaneously the information of conductance and the corresponding force at the junction.[20,21] There are other SPM-based approaches that do not emphasize the occurrence of tip-substrate contact prior to the junction formation, such as *I*(s) with the tip position being lifted from a pre-defined tip-substrate distance[15,22] and *I*(t) with the tip-substrate distance maintained constant[22-24] or coupled with a sinusoidal motion.[25]

Figure 1d shows a three-electrode platform of single molecular transistors (SMTs), originally fabricated for cadmium selenide nanocrystals.[26] A narrow metal film, generally prepared by *e*-beam lithography, is placed on an insulating layer of SiO_2 or Al_2O_3 under which is the gate electrode. By applying a bias to the termini of the metal film, the source-drain junction is created by electromigration in which a cascading collision takes place to dissipate the momentum of the electrons and ions generated under a large electric field.[27] The method to prepare a well-defined junction is still unavailable and it is difficult to obtain an SMT device. Nevertheless, in terms of the electrical characteristics of the molecules, SMTs offer a comprehensive view because the molecular energy levels and their alignment with the Fermi levels of source/drain electrodes can be tuned by the gated potentials.

Electron transporting mechanisms

Table 1 lists four mechanisms of electric transport, including hopping, thermionic emission, direct tunneling, and field emission. The accompanied equations and schemes indicate how the current is a function of the bias voltage (V), temperature (T), and the interelectrode distance (d).

Hopping describes the movement of thermally activated electrons which hop site-by-site through the isolated states across the molecular junction. During the process, the electrons might be localized at some positions within the molecule, particularly for long ones. The phase term which defines the wavefunction of electron changes and thus hopping conduction is an incoherent mechanism. For thermionic emission (Schottky emission), a higher temperature provides the electrons a larger kinetic energy to escape from the electrode surface. The potential barrier to overcome for the escaped electron is the work function of the electrode. The escape leaves in the electrode a positive image charge which exerts an image potential and consequently alters the barrier height. There is a correction term described by the voltage on the exponential term (Table 1), meaning that an increase of the bias voltage reduces the potential barrier and hence increases the current. A larger bias voltage contributes a stronger electric field to draw a larger current across the junction. The applied bias also changes the effect of image force on the potential barrier. Note that the equation for hopping conduction does not have this voltage factor on the exponential term. While hopping and thermionic emission are both temperature-dependent, the magnitude of barrier height determines which pathway is dominant. Specifically, for those with the potential barrier too high to be excited over, hopping is favorable. For cases with small barrier heights, large applied voltages, and high temperatures, the dominant mechanism is likely thermionic emission.

Table 1. Possible conduction mechanisms[28,29]

Mechanism	*I*–V behavior	Schematic diagram[a]
hopping	$I \sim V exp(-E_a/k_BT)$ $I \sim V$ $\ln(I/V) \sim 1/T$	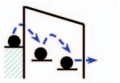
thermionic emission[b] (Schottky emission)	$I \sim T^2 exp\{[A+B(V/d)^{1/2}]/k_BT\}$ $\ln(I) \sim V^{1/2}$ $\ln(I/T^2) \sim 1/T$	
direct tunneling (super-exchange)	$I \sim V exp(-d)$ $I \sim V$ $\ln(I/V) \sim d$	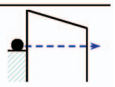
field emission[b] (Fowler-Nordheim tunneling)	$I \sim V^2 exp(-Cd/V)$ $\ln(I/V^2) \sim 1/V$	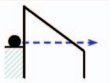

[a] The schemes are adapted from ref 28. [b] A, B, and C are employed to simplify the equation to better show the dependence of parameters T, V, and d. $A = -\phi$, $B = -\frac{1}{2}q^{3/2}(\pi\varepsilon)^{-1/2}$, $C = 4(2m)^{1/2}\phi^{3/2}(3q\hbar)^{-1}$. ϕ, q, ε, m, and $\hbar$ denote, respectively, the barrier height, charge of an electron, dielectric constant, mass of an electron, and Planck's constant.

While the currents of hopping and thermionic emission strongly depend on temperature, those arising from direct tunneling and field emission are insensitive to temperature. For the latter two, the current is a function of interelectrode distance, which is correlated to the molecular length. Direct tunneling takes place at bias voltages smaller than the barrier height with a shape of rectangle or trapezoid. This is the super-exchange process of the Marcus/Hush theory that the tunneling is through the same molecular level and the molecule remains at the ground state.[30] When the bias is larger than the barrier height, the barrier becomes triangle and field emission (*i.e.*, Fowler-Nordheim tunneling) occurs.

Transition between hopping and direct tunneling. The equations in Table 1 show that the dominant conduc-

tion pathway will change, depending on conditions of temperature, bias potential, and the electron transporting distance. Figure 2 elucidates how the transition temperature between hopping and direct tunneling is found. Allara's group acquired *I*-V curves from room temperature to 13 K for 1-nitro-2,5-di(phenylethynyl-4′-mercapto)benzene (see Panel a) in MMM junctions created by electromigration.[31,32] To examine the effect of temperature, the current values are plotted against 1/T (Arrhenius equation, Figure 2b). The upper axis indicates the temperature. At the same temperature, the data points going vertically upwards are obtained at larger bias potentials. The solid lines connect the data points with the same bias. There are temperature dependent and independent segments, ascribed to hopping at higher temperatures and to direct tunneling at the lower ones, respectively. The transition temperature, T_{trans}, is determined at where the two segments intersect. For a larger bias, T_{trans} becomes smaller. This is attributed to (1) reduced activation energy (E_a, see Table 1) and (2) bias-induced heat dissipation under a larger applied potential, making electron overcome the energy barrier at lower temperatures.

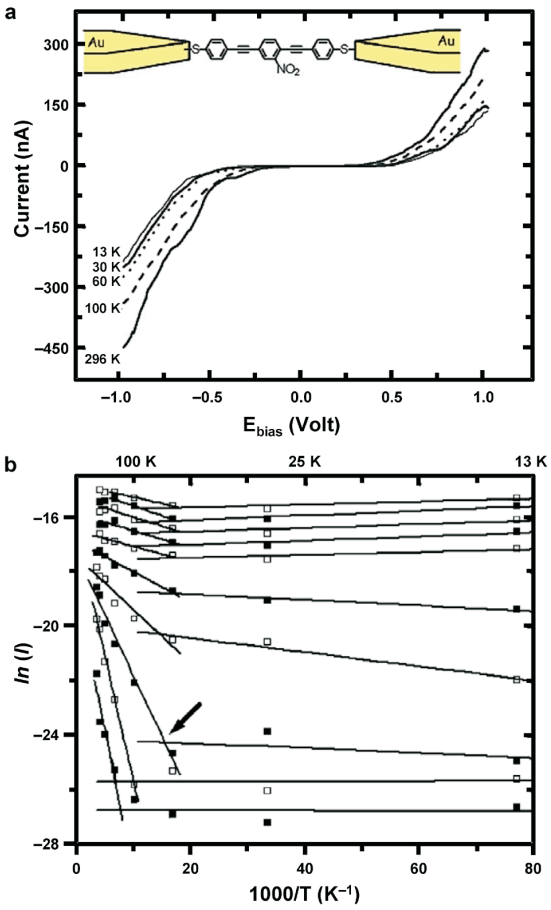

Fig. 2. Temperature-dependent hopping-tunneling transition.[31] (a) *I*–V curves at various temperatures and (b) the corresponding Arrhenius plots. As the temperature decreases (see upper axis), the measured conductance decreases and the conduction pathway changes from hopping (temperature-dependent) to direct tunneling (insensitive to temperature change). The arrow indicates the transition temperature (T_{trans}). For each temperature, displayed are 10 data points which, starting from the bottom, are 0.1 ~ 1.0 V with an interval of 0.1 V. Adapted with the permission from ref 31, copyright 2004, American Chemical Society.

In addition to temperature, the increase of the molecular length, d, leads to a mechanistic transition from direct tunneling to hopping conduction. In a cAFM study by Choi and Frisbie,[14] the monolayer resistance was measured for a homologous series of OTPI*n* (oligo-tetrathiafulvalene pyromellitic diimide-imine, Figure 3a). For short oligomers, OTPI1~OTPI3, the decay constant (β) is 2.5 nm^{-1}, significantly larger than that of the longer oligomers ($n \geq 4$, $d > 7$ nm). Figure 3b demonstrates that OTPI1 is temperature-independent while the longer ones (*e.g.*, OTPI3 and OTPI6) are temperature-dependent, consistent with the characteristics of tunneling and hopping conduction. Similar behaviors have been found for conjugated oligophenyleneimines.[13]

Thermionic emission and direct tunneling. Figure 4 shows an example of the transition between thermionic emission and tunneling, reported by Mirkin and co-workers.[33] A free-standing nanogap is fabricated by lithography. The MMM junctions contain α,ω-dithiol terminated oligo(phenylene ethynylene) (OPE). The current decreases with a decreasing temperature and becomes insensitive to temperature, similar to hopping-direct tunneling transition in Figure 2. However, the authors suggest that thermionic emission is a more suitable mechanism to describe the current behavior than hopping because of the linear relationship between $ln(I)$ and $V^{1/2}$ (Figure 4c and Table 1).

Direct tunneling and Fowler-Nordheim tunneling. There are quite a few examples of the transition between direct tunneling and Fowler-Nordheim tunneling (F-N tunneling, also called field emission).[34] The transport pathway is influenced by the magnitude of the applied bias which changes the shape of potential barriers. The potential barriers sketched in the upper portion of Figure 5 and the vertical dashed line illustrate how the transition voltage (V_{trans})

is determined.[12] The barrier height is resulted from the energy difference between the Fermi level of electrodes (E_{Fermi}) and the energy levels of frontier molecular orbitals (E_{FMO}; E_{HOMO} or E_{LUMO}, energy levels of the highest occupied molecular orbital or the lowest unoccupied molecular orbital). When the bias becomes larger than V_{trans}, electrons overcome the energy barrier more easily, leading to a larger conductance. In the cAFM study of Frisbie, Kushmerick, and co-workers,[12] the effect of barrier heights are examined by monolayers of aromatic monothiols. The values of V_{trans} are found linearly correlated to the energy difference of

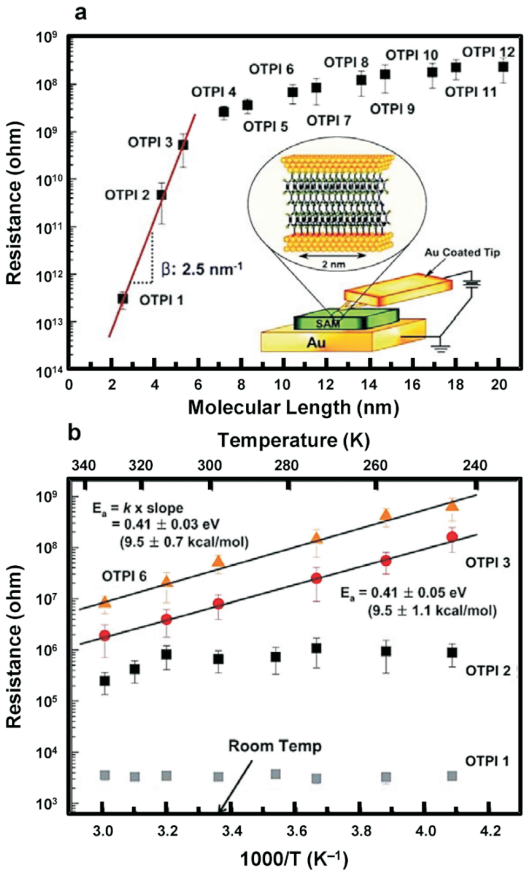

Fig. 3. Molecular length-dependent hopping-tunneling transition.[14] Resistance plotted with the logarithmic scale against (a) molecular length and (b) the reciprocal of temperature. The resistance of molecular junctions increases rapidly for short oligomers (OTPI1~OTPI3, oligotetrathiafulvalene pyromellitic diimide-imine) and slower for those with repeated unit larger than 4. The resistance for OTPIs is insensitive to temperature for OTPI1 and is temperature-dependent for those longer than OPTI2, indicative of a transition of mechanism from tunneling to hopping. Adapted with the permission from ref 14, copyright 2010, American Chemical Society.

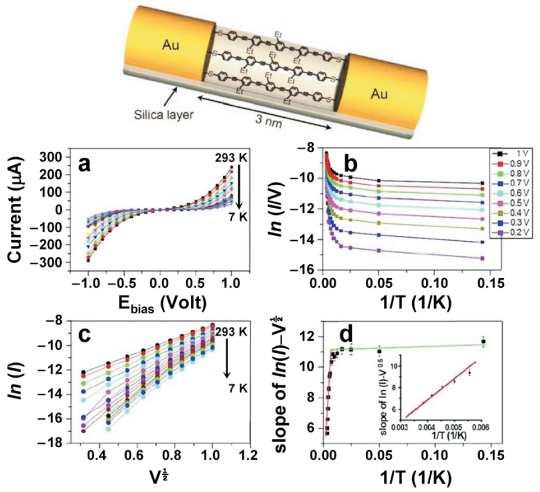

Fig. 4. Temperature-dependent transition between thermionic emission and direct tunneling.[33] (a) *I*–V curves at various temperatures, (b) the corresponding Arrhenius plots of *lnG*, (c) linear correlation between *ln*(*I*) and $V^{1/2}$, (d) a temperature-dependent plot of the slopes derived in Panel c. Panels c and d suggest that at high temperatures (T > 120 K) thermionic emission describes the conduction of OPEs better than hopping. Adapted with the permission from ref 33, copyright 2008, American Chemical Society.

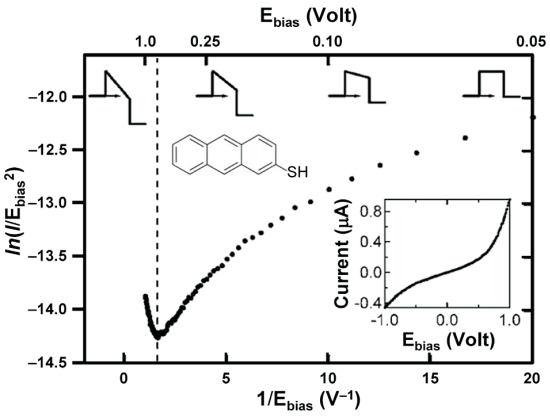

Fig. 5. Bias-dependent transition between direct tunneling and F-N tunneling.[12] The vertical dashed line indicates where the transition takes place for Au-anthracenethiol-Au junctions. The insets at upper portion show the barrier height as a function of the applied bias. The inset at the lower-right part shows the I-V curve of the molecular junction. Adapted with the permission from ref 12, copyright 2006, American Physical Society.

(E_{Fermi} – E_{HOMO}). Figure 5 is obtained from a monothiol Au-anthracenethiol-Au junction. The *I*-V curve is asymmetric and V_{trans} is dependent on bias polarity because one of the metal-molecule interfaces is through sulfur-gold interactions and the other is *via* physical contact.

Displayed in Figure 6 is an SMT study[35] which demonstrates that the transition between direct tunneling and F-N tunneling can be adjusted by the electric field applied at the gate electrode. For example, the HOMO-LUMO gap of saturated octanedithiol is so large that the V_{trans} is absent in typical bias ranges for *I*–V sweeping (the bottom curve of Panel a). The drawings at the right of Panel b illustrate the effect of V_{Gate}. Specifically, Points B and C and the connected dashed line indicate where the V_{trans} occurs. Those being subjected to stronger field effects bear smaller barrier heights (*e.g.*, those toward Point C) thus exhibit smaller values of V_{trans}. The barrier heights are depicted as the depth of the triangular potential well, equivalent to the lengths of the vertical double arrows at Points B and C. This example shows that the gate voltage can tune molecu-

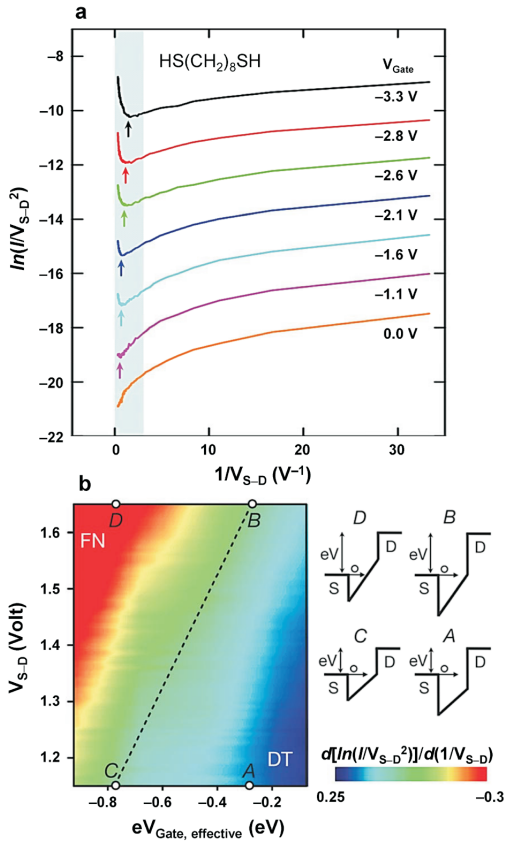

Fig. 6. Electric field-gated transition between direct tunneling and F-N tunneling. (a) F-N plots of *I*–$V_{S–D}$ curves recorded as a function of gate voltage.[35] The *x*-axis is the applied bias voltage which in SMTs is the energy difference between the source and drain electrodes. V_{trans}, indicated by arrows, is modulated by the gate voltage. (b) 2D conductance map. The *x*- and *y*-axes are effective gate voltage ($eV_{G,eff}$) and source-drain bias ($V_{S–D}$), respectively. The effective gate voltage, $V_{G,eff}$, is determined by $V_{G,eff} = |\alpha|V_G$, where α is the gate efficiency factor which describes the effectiveness of molecular orbital gating by $\alpha = \Delta V_{trans}/\Delta V_G$. The insets at right illustrate the effect of gate voltage on barrier height. DT and FN stand for direct tunneling and Fowler-Nordheim tunneling, respectively. Adapted with the permission from ref 35, copyright 2009, Macmillan Publisher Ltd.

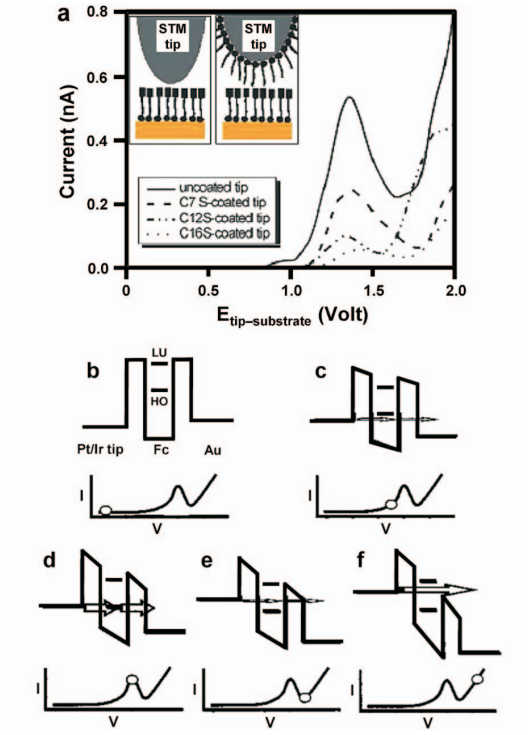

Fig. 7. Energy level alignment between the electrode E_{Fermi} and E_{FMO} of ferrocene (Fc).[36,37] (a) Experimental schemes and spectra of the tunneling spectroscopy. Although the current attenuates with the modification of alkanethiol monolayers at the tip, the peak position remains unaffected. (b~f) A proposed mechanism for the *I*–V characteristics of negative differential resistance. The peak at 1.4 V is attributed to the resonant tunneling in which electrons transport *via* the HOMO level of Fc (Panel d). Adapted with the permission from refs 36 and 37, copyright 2001 and 2004, American Chemical Society.

lar E_{FMO} relative to E_{Fermi}.

From direct tunneling to resonant tunneling. Figure 7a, reported by Gorman *et al.*,[36,37] shows characteristics of NDR (negative differential resistance) in which regime, contradictory to the Ohmic law, the current decreases with an increase bias voltage. The experiments were carried out by scanning tunneling spectroscopy on monolayers of ferrocene-tagged alkanethiolates. The *I*-V curves were obtained with bare and alkanethiol-coated tips. The latter cases render thicker tunneling barriers and result in smaller current.[37] Electron transporting mechanisms associated with direct tunneling and resonant tunneling are proposed to explain NDR. With a double-barrier model in which the FMOs of ferrocene moiety are sandwiched by the alkane insulating layers, Panels b~f elaborate a possible mechanism.

Panels b and c describe that the current increases with the decrease of the $|E_{Fermi} - E_{FMO}|$ gap and the dominant conduction pathway goes from direct tunneling to field emission.[36] Panel d illustrates the alignment between energy levels of E_{Fermi} and E_{FMO} of ferrocenyl moiety (*i.e.*, resonant tunneling). When it becomes off-resonant at an even higher potential (Panel e), the current begins to drop. Panel e illustrates thermionic emission for the bias large enough to overcome the barrier height. It should be noted that, although off-on-off resonant tunneling may give rise to NDR characteristics,[38,39] there are other possibilities, such as a conformational change of molecular structures,[40] redox events,[41] and the polaron formation caused from the interactions between electrons and vibrational modes of molecules.[42]

Mechanisms manifested by single-molecule transistors

Figure 6 demonstrates that SMTs offer rich information on electron transport. The gate electrode interacts with the molecules via an insulating layer. Such an electrostatic or capacitive coupling allows the gate to tune the molecular energy levels (*e.g.*, electron states from n to n+1) relative to the electrode E_{Fermi} *via* the applied gate voltage (V_G). Mapped by Tour, Natelson, and co-workers,[43] Figure 8 illustrates what the conductance data from SMTs look like (Panel b) and the possible transport pathways. The 3D contour of $\partial I_{S-D}/\partial V_{S-D}$ is generated by measuring currents as a function of source-drain bias (V_{S-D}, *y*-axis) at the corresponding V_G (*x*-axis).

In Panel b of Figure 8, numbers 1~5 denote examples of transporting pathways. Point 1 resides in the dark regime, indicative of no current or a very small conductance value of $\partial I_{S-D}/\partial V_{S-D}$. The transport is suppressed by Coulomb blockade. For a system bearing a very small capacitance (*C*), Coulomb charging energy ($E_C = e^2/2C$) becomes significant and quantized. The number of electrons is fixed unless the barrier of charging energy is overcome. Points 1 and 1' of Panel c depict that the transport is *via* mechanisms of "super-exchange" or "elastic co-tunneling" such that the total number of electrons remains unchanged.

Point 2 represents "*inelastic* co-tunneling" in which the electron is filled into an excited vibrational level (E_{vib}: the dotted lines in Panel c). Point 3 takes place at a higher V_{S-D} where the electron overcomes the charging energy arising from Coulomb blockade. The electrode E_{Fermi} is aligned with the molecular level, leading to a higher trans-

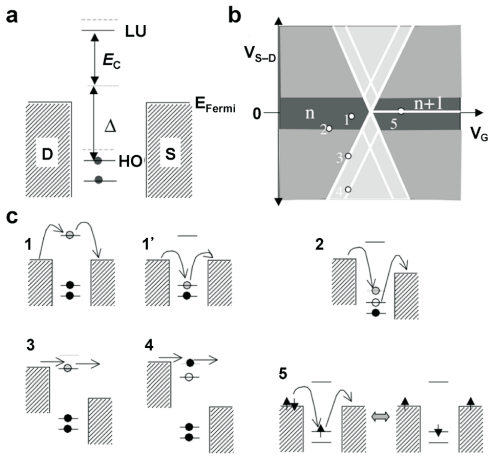

Fig. 8. Electronic transporting mechanisms revealed by SMTs.[43] (a) Energy levels of molecules in a single-electron transistor. D: drain electrode; S: source electrode; Δ: $|E_{HOMO} - E_{LUMO}|$ or single-particle level spacing; E_C: Coulomb charging energy; dotted levels: vibrational excitations in molecular devices. The energy required to excite an electron from HOMO to LUMO is the sum of the single-particle level spacing and Coulomb blockade charging energy (*i.e.*, $\Delta + E_C$), also termed addition energy. (b) A 3D-contour of $\partial I_{S-D}/\partial V_{S-D}$ (brightness) as a function of V_G and V_{S-D}. The transition from n to n + 1 represents one-electron reduction on the molecule. Numbers 1~5 on the map correspond to mechanisms illustrated in Panel c.[43] (c) Conduction processes associated with V_G, V_{S-D}, and electronic levels of the molecule. 1: elastic tunneling; 2: inelastic tunneling (IET); 3: resonant conduction; 4: resonant inelastic tunneling (RIET); 5: Kondo resonant conduction. Adapted with the permission from ref 43, copyright 2004, American Physical Society.

porting efficiency (*viz.*, resonant tunneling). In the 3D conductance map, the events of resonant tunneling encompass a rhombic and dark regime called Coulomb diamonds. The slopes of the diamond vary from one device to another, dependent on the degree of molecule-electrode coupling. The magnitude of the energy difference between neighboring electronic levels can be estimated by the V_{S-D} values required to reach the vertex from the center of the diamond. The vertices along the V_G axis describe where the Coulomb blockade vanishes and the total energy is the same for molecules carrying charges of n and n+1. Hence, the term "charge degeneracy points" are adapted to describe the vertex, where redox transitions take place.

Point 4 shows an example of RIET (resonant inelastic tunneling) in which the electron transport is mediated by an additional resonant vibrational state. Note that Points 2 and 4 are both inelastic events associated with vibrational levels yet the former does not require the alignment of E_{Fermi} with those of the vibrational levels. The process is termed IET (inelastic tunneling). When the energy of the injected electron is larger than the energy difference between the ground state and a vibrational state, a small fraction of the electrons can excite the vibrational mode at the expense of losing energy. The opening of an IET channel raises the tunneling efficiency. The increased current is proportional to the excess energy (*i.e.*, the applied bias) and thus, on the conductance map ($\partial I/\partial V$), the regime appears constant after V_{S-D} is greater than what corresponds to the energy of a vibrational mode.[44] In principle, all vibrational modes are observable.[45,46] However, not all modes are found in a measurement and the spectra varies from one device to another because the excited modes are strongly affected by local molecule-electrode configurations.[47]

Point 5 corresponds to the Kondo regime for those with unpaired spins. Kondo resonance exhibits a sharp conductance peak near zero V_{S-D} at low temperatures. The resonance arises from a new state, developed *via* a many-body phenomenon, involving the exchange between the unpaired electrons on the molecule and electrons in the electrodes. The electron transport is presumably frustrated by the large energy barrier of $|E_{Fermi} - E_{FMO}|$. Intriguingly, the Heisenberg uncertainty principle opens a short time of $h/|E_{Fermi} - E_{FMO}|$, available for the trapped unpaired electron to escape. To keep the number of charge unchanged, another electron with the opposite spin from the electrode sits on the molecule within the timeframe. The elastic co-tunneling process takes place many times from different conducting electrons such that a new density of state is created at E_{Fermi}. This is a higher order tunneling process developed at low temperatures under which conditions the exchange events of free electrons from electrodes develop a polarization to screen the magnetic moment of the unpaired spin at the junction.[48,49] Panel c5 illustrates that the up-spin electron on the molecule is replaced by a down-spin one which comes from the drain electrode.

The degree of coupling strength between the elec-

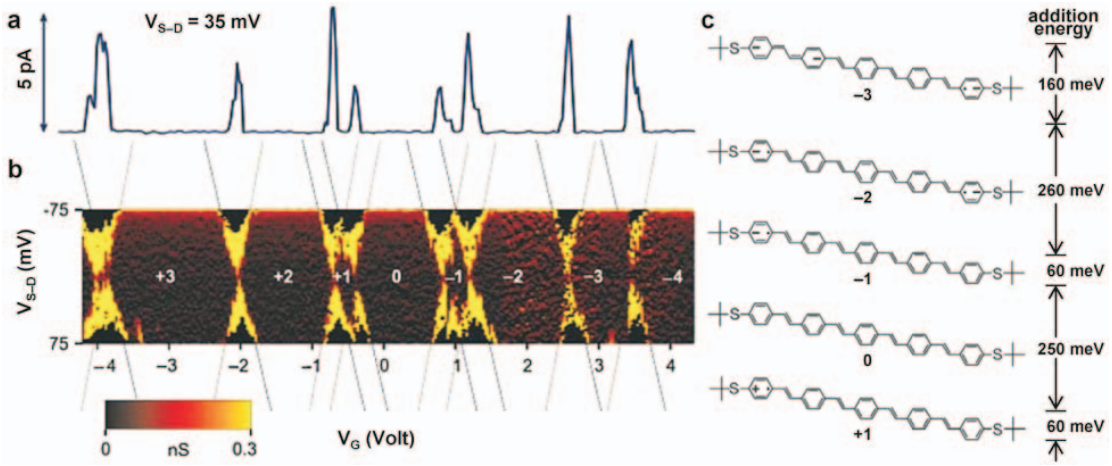

Fig. 9. Transition of OPV5 across eight electronic levels.[51] (a) A representative I_{S-D} traces plotted against V_G, obtained at the indicated V_{S-D} bias. (b) Conductance map. The dark and bright areas are regions of Coulomb blockade and resonant tunneling, respectively. (c) Selected redox states of OPV5 and the corresponding addition energies. The numbers in the map indicate the charge carried on the molecule.[51] The experiments used an aluminum oxide (~5-nm)/aluminum gate electrode and were conducted at 4.2 K. Adapted with the permission from ref 51, copyright 2003, Macmillan Publisher Ltd.

trons in the electrodes and those in the molecule decides the features of the conductance map. For the weak coupling cases, Coulomb diamonds appear featurelessly dark and only electronic levels are observed. For those with strong coupling, a coherent one-step electron transport is more favorable than a two-step process such as hopping. The energy levels of the molecules are broadened such that $|E_{Fermi} - E_{FMO}|$ is reduced and I_{S-D} becomes less dependent on V_G. In the intermediate coupling cases, the conductance map unveils mechanisms involving electron-electron correlation, such as co-tunneling, IET, and Kondo resonance. For devices with the molecule bearing different coupling strengths with the two electrodes, the slopes of the diamond shapes become asymmetric.[50] The following literature examples illustrate these mechanisms.

Transport involving electronic levels: n → n+1. Figure 9 presents an SMT study by Bjørnholm *et al.* who unravels multiple electronic levels of a conjugated oligophenylenevinylene, OPV5.[51] Panel a shows that, at a fixed V_{S-D}, the current exhibits alternative characteristics of Coulomb blockade and conductive regimes along the V_G axis. The conductance map displays electronic levels of eight electrostatic charges although most Coulomb diamonds are incomplete. The slopes of the diamond boundaries are in parallel, suggesting that there is only one set of molecule-electrode coupling and hence one single molecule present at the SMT junction.

Figure 9c lists the energy required to promote to the next oxidation state for OPV5, estimated from the V_{S-D} at the vertices of the Coulomb diamonds.[51] The values are far smaller than 2.5 eV extracted from the absorption spectrum (450 nm) in solution. Based on simulation results of a Hubbard model, the difference is likely due to the formation of electrostatic image charges at the source and drain electrodes. The image charges stabilize the charge trapped on the molecule and, therefore, perturb significantly the electronic levels of OPV5. With a gated MCBJ setup, van der Zant and coworkers[7] demonstrated the presence and the effect of image charges for a zinc porphyrin. The excellent control over the interelectrode spacing by MCBJ allows the fine tuning of the induced image charges. With the additional gate electrode, the shifts of E_{FMO} relative to E_{Fermi} can be determined and are found dependent reversibly on the distance between electrodes, consistent with the image-charge effect. The shifts of several hundreds of meV are reported for the electrode movement within a few angstroms. Hybrid states between electrodes and the Zn porphyrin are proposed. These results suggest that the conductance behavior at molecular junctions involves molecule-electrode interactions, distinctly different than what is expected from FMOs of free molecules.

Vibration-assistant tunneling: RIET and IETS. Similar to resonant tunneling, resonant inelastic tunneling (RIET) is facilitated by a discrete state which, however, involves molecular vibrations. The conductance map in Figure 10 shows features of RIET for an SMT containing a tricopper complex in which the metal centers are collinear and coordinated by four equatorial ligands of tripyridylamido anion.[52,53] There are three charge states defined by Coulomb diamonds (dark area). At the region outside the Coulomb diamonds, there are additional bright lines in parallel to the boundaries of diamonds. For example, in the N state at V_G of *ca.* 50 V, there are conductance lines starting

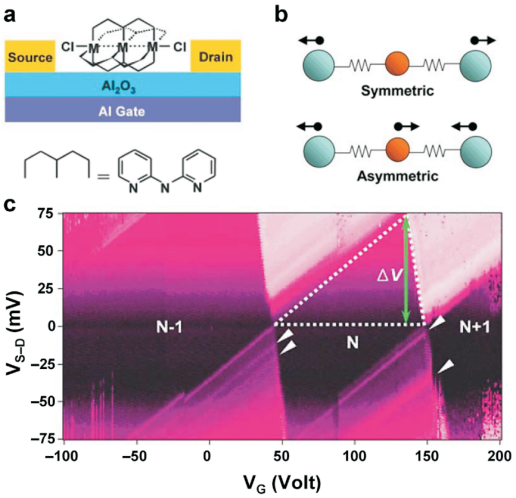

Fig. 10. Vibration-assistant conductance for a linear tricopper complex.[53] (a) Scheme of an SMT and the molecular structure. (b) Mass-spring models of symmetric and asymmetric vibrational modes. There are two types of effective masses with the termini heavier than the inner one. The effective mass for the central one contains one copper atom, four nitrogen atoms, and one-third of total carbon and hydrogen atoms. The terminal ones consist of the same atoms and an additional chlorine atom. (c) Conductance map. The white triangles mark excitations at V_{S-D} of 12.5, 20.5 mV and at 5, 33 mV in the N and N + 1 electron states, respectively. The experiments were carried out at 4.2 K. Adapted with the permission from ref 53, copyright 2006, American Chemical Society.

from 12.5 and 20.5 mV, attributed to symmetric and asymmetric stretching modes, respectively (Panel b). In the N+1 state, the RIET lines are observed at different V_{S-D} because the molecular structure and the excess energies needed to excite the vibrations are changed with the molecular oxidation state.

Figure 11 represents an interesting case with strong molecule-electrode interactions which yield vibration-like behaviors of mechanical oscillation excited by the transporting electrons. The conductance maps of single C_{60} are from four SMT devices by McEuen and coworkers.[52,53] The RIET lines are indicated by the white triangles pointing at V_{S-D} of 3~7 mV. The values are commonly observed in different charge states. Therefore, these lines are unlikely the intrinsic vibrational modes of C_{60}. In addition, the intrinsic vibrational modes such as that of Panel e are expected to take place at a larger V_{S-D}. Hence, deformational vibrations of C_{60} are unaccounted for the RIET features.

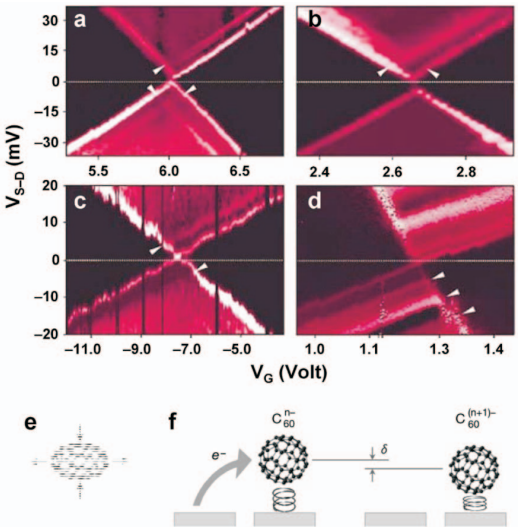

Fig. 11. Conductance maps of C_{60} SMTs and proposed RIET mechanisms.[52] (a-d) Conductance maps obtained from four SMT devices. At the intercept of conductance gaps, there are white triangles pointing to RIET lines. (e) An example of internal vibrational modes of C_{60}. The expected energy quantum for this mode is about 35 mV. (f) Illustration of the center-of-mass oscillation. The C_{60}–gold interactions provide the spring constant of a harmonic oscillation. The scheme depicts that the addition of an electron activates the attractive interaction with the positive image charge at the metal electrode. δ: quantized movement excited by the excess energy of the electron. Adapted with the permission from ref 52, copyright 2000, Macmillan Publisher Ltd.

Panel f displays the proposed model of the center-of-mass oscillation for C_{60} on gold electrodes. The C_{60}-gold adsorption is about 1 eV,[52,53] strong enough for the C_{60} to withstand the bouncing motion. A force constant of ~70 N/m, a vibrational frequency of 1.2 THz, and a quantized vibrational energy of 5 meV are derived, consistent with the observed RIET. The equal spacing of 5 mV for the multiple RIET lines in Panel d also supports the model of harmonic motion. In summary, for electrons carrying an excess energy of ~5 meV, the spontaneous emission of this energy starts the oscillation of C_{60} and the current flows.

Inelastic electron tunneling spectroscopy (IETS) was introduced by Jaklevic and Lambe in 1966 with acetic acid or propionic acid embedded in metal-oxide-metal junctions, in which the signatures corresponding to the molecular vibrational modes were excited by the applied bias potential.[54] The transport process does not involve the transition between electronic levels and the current is low. To manifest the vibration-assistant transport, the spectra are presented by plots of d^2I/dV^2 which are experimentally acquired typically using a phase lock-in device incorporated with a small sinusoidal modulation. Mathematical treatment from *I*–V curves cannot provide satisfactory data quality due to the low signal-to-noise level.

Panels a and b of Figure 12 are obtained from SMTs of octanedithiol and benzenedithiol, respectively, exemplifying molecules with a large and relatively small HOMO/LUMO gaps.[35] The characteristic peak positions provide unambiguous evidence to confirm that the conductance maps of SMTs are results of electron transport through the target molecules. The two molecules respond very differently to the gating effect. Octanedithiol has a large HOMO/LUMO gap and thus the value of $|E_{Fermi} - E_{FMO}|$ is unaffected by the applied gate voltage. For benzenedithiol, with the effective gate voltage going from 0 to –0.66 V, peak intensities of vibrations associated with the benzene moiety increase preferentially by 40 folds (see the *y*-axis at the right). In contrast, the intensity of Au-S vibration does not change (see the *y*-axis at the left). The drawings at the right of Panel b illustrate that a more negative gate voltage drives the HOMO closer to E_{Fermi}. The near-resonant conditions boost the tunneling efficiency.

Transport involving electron spin: Kondo resonance. Kondo effect was first discovered in bulk metal

whose zero-bias conductance decreases with lowering temperature but increases significantly at an extremely low temperature. The origin was then verified to the magnetic impurity.[48,49,55] Kondo resonance has been observed for

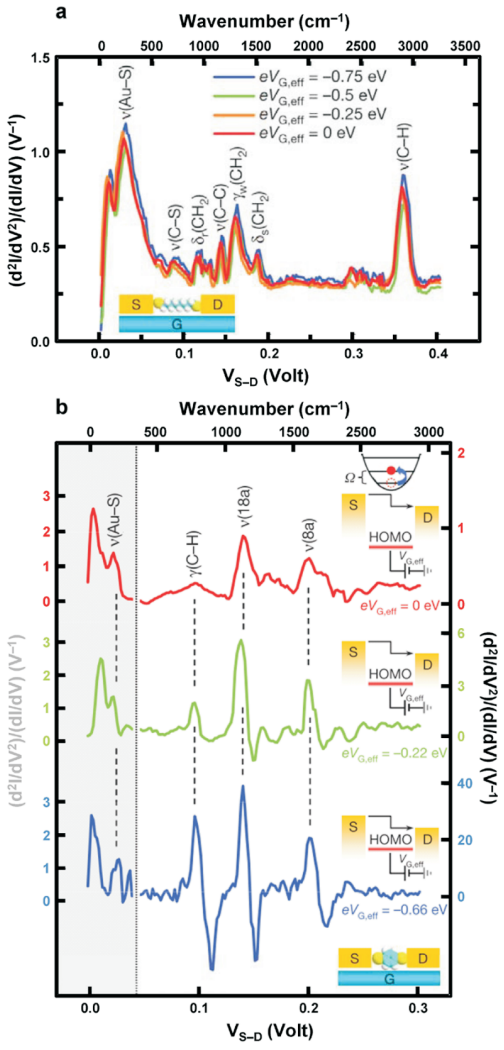

Fig. 12. Gating effect on IETS of (a) octanedithiol and (b) benzenedithiol.[35] The spectra of octanedithiol are unaffected by the gating yet some vibration modes of benzenedithiol respond significantly. Insets depict near-resonant electron transport. For Panel b, the gate efficiency factor α is +0.22, obtained by $\alpha = \Delta V_{trans}/\Delta V_G$. The positive sign shows the transport is mediated by the HOMO. In Panel b, the peak intensity in the shaded area (< 45 mV or 363 cm^{-1}) is referred to the left axis and the rest to the right axis. Conditions: gold source and drain electrodes, a ~3 nm Al_2O_3 dielectric layer on Al electrode; temperature, 4.2 K. Adapted with the permission from ref 35, copyright 2009, Macmillan Publisher Ltd.

C_{60},[56] organometallics,[57,58] a cobalt porphyrin,[59] atomic-scale gold clusters,[60] and a single arsenic atom.[61] Figures 13 and 14 are the earliest SMT examples of Kondo resonance.[57,58]

Park and co-workers use a divanadium molecule, V_2, to provide the unpaired spin at the junction.[57] Electrochemical studies observe 3 accessible oxidation states, including V_2^-, neutral form V_2^0, and V_2^+. In the neutral form, each vanadium atom is +4 and carries one *d*-electron. Magnetic measurements show that the ground states of V_2^- and V_2^0 are a spin-singlet (S = 0) and a spin-quadruplet (S = 3/2),

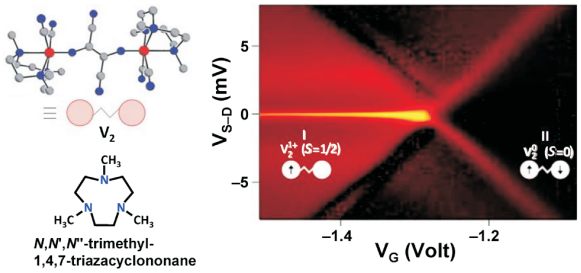

Fig. 13. Kondo resonance observed from an SMT containing a divanadium complex.[57] The experiments were conducted at 0.3 K. The devices use gold source and drain electrodes and an alumina gate under a ~3-nm-thick insulating layer of Al_2O_3. The colors of red, gray, and blue stand for atoms of vanadium, carbon, and nitrogen. The ligand structure is also provided. Adapted with the permission from ref 57, copyright 2002, Macmillan Publisher Ltd.

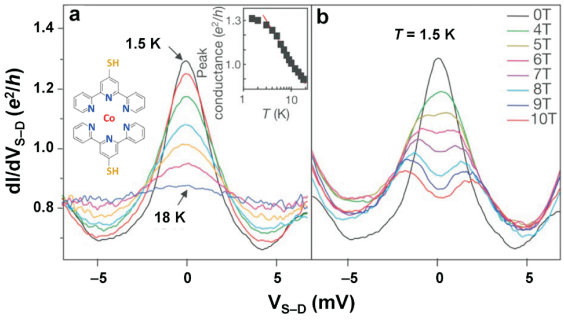

Fig. 14. The Kondo resonance is a function of (a) temperature and (b) the strength of magnetic field.[58] The inset shows that zero-bias conductance decreases logarithmically with temperature. For this particular device, the peak becomes insignificant at 18 K. The devices use gold source and drain electrodes. The insulating layer is 30-nm-thick SiO_2 and the gate electrode is a doped Si substrate. Adapted with the permission from ref 58, copyright 2002, Macmillan Publisher Ltd.

respectively. For V_2^+, it has only one *d*-electron left and is a spin-doublet (S = 1/2). The conductance map (Figure 13) shows a charge degeneracy point where V_2^0 and V_2^+ have the same energy. A sharp conductance peak at zero bias is present in region I and absent in region II, consistent with the behavior of Kondo resonance.

Dependence on temperature and applied magnetic field is the signature of Kondo resonance arising from a single spin (S = 1/2). Figure 14 demonstrates the strength of Kondo resonance as a function of temperature and magnetic field for a cobalt complex.[58] The selection of this molecule is due to the accessible redox potential for $Co^{2+/3+}$. The spin quantum number of the ground state is S = 1/2 for Co^{2+} ($3d^7$) and S = 0 for Co^{3+} ($3d^6$). Panel a and the inset show that the Kondo resonance becomes more pronounce at lower temperatures. Displayed in Panel b is the Zeeman effect[62] that the energy levels of spin-up and spin-down states split under a magnetic field. The difference in V_{S-D} between the split peaks is twice the Zeeman effect. Also examined in the study is another cobalt complex with linkers of $-(CH_2)_5-$ attached between the thiol and pyridyl groups. SMT Devices of this longer complex exhibit smaller conductance and the Kondo resonance is not found. The results suggest that the electrode-molecule coupling is weak and intermediate for the long and short cobalt complexes, respectively.

CONCLUDING REMARKS

The electron transport through molecule-scale devices receives intensive interests both theoretically and experimentally. The contemporary development of experimental schemes has made the measurements more accessible and better defined. The conductance data at the molecular level from collective efforts in this field allow the elucidation of the underlying physics and chemistry. In this review, fundamental mechanisms of electron transport in molecular junctions are introduced. The emphasis is on conditions which yield a favorable conduction pathway over others and on parameters that control the transition between mechanisms. For example, hopping could be dominant in the cases of high temperature, long molecules, or weak electrode-molecule coupling. Under a higher voltage, the thermionic emission could be a more facile mechanism than hopping. In practice, the observed conductance is a mixed behavior from many possible pathways. There are experimental results remained difficult to explain by simple models. At the present stage for single-molecule studies, most two-terminal MMM junctions offer transitory structures of molecular conformation and the headgroup-electrode contact geometries. The fabrication of three-electrode SMTs suffers low successful rates. Efforts in devising measurement platforms that can provide stable and reproducible MMM structures at the atomic level will result in detailed understanding to further advance important aspects of the molecular conductance.

ACKNOWLEDGEMENTS

The authors thank Dr. M.-J. Huang and Mr. P.-C. Liu for the preparation of this manuscript and thank National Science Council for the financial support.

REFERENCES

1. Aviram, A.; Ratner, M. A. *Chem. Phys. Lett.* **1974**, *29*, 277-283.
2. Kiguchi, M.; Kaneko, S. *Phys. Chem. Chem. Phys.* **2013**, *15*, 2253-2267.
3. Aradhya, S. V.; Venkataraman, L. *Nat. Nanotechnol.* **2013**, *8*, 399-410.
4. Cuevas, J. C.; Scheer, E. *Molecular Electronics: An Introduction to Theory and Experiment*; World Scientific: Singapore, 2010; Vol. 1.
5. Moreland, J.; Ekin, J. W. *J. Appl. Phys.* **1985**, *58*, 3888.
6. Reed, M. A.; Zhou, C.; Muller, C. J.; Burgin, T. P.; Tour, J. M. *Science* **1997**, *278*, 252-254.
7. Perrin, M. L.; Verzijl, C. J. O.; Martin, C. A.; Shaikh, A. J.; Eelkema, R.; van Esch, J. H.; van Ruitenbeek, J. M.; Thijssen, J. M.; van der Zant, H. S. J.; Dulic, D. *Nat. Nanotechnol.* **2013**, *8*, 282-287.
8. Perrin, M. L.; Prins, F.; Martin, C. A.; Shaikh, A. J.; Eelkema, R.; van Esch, J. H.; Briza, T.; Kaplanek, R.; Kral, V.; van Ruitenbeek, J. M.; van der Zant, H. S. J.; Dulic, D. *Angew. Chem. Int. Ed.* **2011**, *50*, 11223-11226.
9. Cui, X. D.; Primak, A.; Zarate, X.; Tomfohr, J.; Sankey, O. F.; Moore, A. L.; Moore, T. A.; Gust, D.; Harris, G.; Lindsay, S. M. *Science* **2001**, *19*, 571-574.
10. Chen, I-W. P.; Fu, M.-D.; Tseng, W.-H.; Yu, J.-Y.; Wu, S.-H.; Ku, C.-J.; Chen, C.-h.; Peng, S.-M. *Angew. Chem. Int. Ed.* **2006**, *45*, 5814-5818.
11. Morita, T.; Lindsay, S. *J. Am. Chem. Soc.* **2007**, *129*, 7262-7263.
12. Beebe, J. M.; Kim, B.; Gadzuk, J. W.; Frisbie, C. D.; Kushmerick, J. G. *Phys. Rev. Lett.* **2006**, *97*, 026801.
13. Choi, S. H.; Kim, B.; Frisbie, C. D. *Science* **2008**, *320*, 1482-1486.
14. Choi, S. H.; Frisbie, C. D. *J. Am. Chem. Soc.* **2010**, *132*,

16191-16201.
15. Song, H.; Lee, H.; Lee, T. *J. Am. Chem. Soc.* **2007**, *129*, 3806-3807.
16. Xu, B.; Tao, N. J. *Science* **2003**, *301*, 1221-1223.
17. Yanson, A. I.; Bollinger, G. R.; van den Brom, H. E.; Agrait, N.; van Ruitenbeek, J. M. *Nature* **1998**, *395*, 783-785.
18. Quek, S. Y.; Kamenetska, M.; Steigerwald, M. L.; Choi, H. J.; Louie, S. G.; Hybertsen, M. S.; Neaton, J. B.; Venkataraman, L. *Nat. Nanotechnol.* **2009**, *4*, 230-234.
19. Moreno-García, P.; Gulcur, M.; Manrique, D. Z.; Pope, T.; Hong, W.; Kaliginedi, V.; Huang, C.; Batsanov, A. S.; Bryce, M. R.; Lambert, C.; Wandlowski, T. *J. Am. Chem. Soc.* **2013**, *135*, 12228-12240.
20. Li, X.; He, J.; Hihath, J.; Xu, B.; Lindsay, S. M.; Tao, N. *J. Am. Chem. Soc.* **2006**, *128*, 2135-2141.
21. Frei, M.; Aradhya, S. V.; Koentopp, M.; Hybertsen, M. S.; Venkataraman, L. *Nano Lett.* **2011**, *11*, 1518-1523.
22. Haiss, W.; Martin, S.; Leary, E.; van Zalinge, H.; Higgins, S. J.; Bouffier, L.; Nichols, R. J. *J. Phys. Chem. C* **2009**, *113*, 5823-5833.
23. Haiss, W.; van Zalinge, H.; Higgins, S. J.; Bethell, D.; Höbenreich, H.; Schiffrin, D. J.; Nichols, R. J. *J. Am. Chem. Soc.* **2003**, *125*, 15294-15295.
24. Chen, I-W. P.; Tseng, W.-H.; Gu, M.-W.; Su, L.-C.; Hsu, C.-H.; Chang, W.-H.; Chen, C.-h. *Angew. Chem. Int. Ed.* **2013**, *52*, 2449-2453.
25. Zhou, J.; Chen, F.; Xu, B. *J. Am. Chem. Soc.* **2009**, *131*, 10439-10446.
26. Klein, D. L.; Roth, R.; Lim, A. K. L.; Alivisatos, A. P.; McEuen, P. L. *Nature* **1997**, *389*, 699-701.
27. Park, H.; Lim, A. K. L.; Alivisatos, A. P. *Appl. Phys. Lett.* **1999**, *75*, 301-303.
28. Chen, J.; Lee, T.; Su, J.; Wang, W.; Reed, M. A.; Rawlett, A. M.; Kozaki, M.; Yao, Y.; Jagessar, R. C.; Dirk, S. M.; Price, D. W.; Tour, J. M.; Grubisha, D. S.; Bennett, D. W. *Molecular Electronic Devices*. In *Molecular Nanoelectronics*, Reed, M. A.; Lee, T., Eds.; American Science Publishers: Stevenson Ranch, CA, 2003; p 89.
29. Cuevas, J. C.; Scheer, E. *Molecular Electronics: An Introduction to Theory and Experiment*; World Scientific: Singapore, 2010; Vol. 1, p 360.
30. Ratner, M. A. *J. Phys. Chem.* **1990**, *94*, 4877-4883.
31. Selzer, Y.; Cabassi, M. A.; Mayer, T. S.; Allara, D. L. *J. Am. Chem. Soc.* **2004**, *126*, 4052-4053.
32. Selzer, Y.; Cai, L.; Cabassi, M. A.; Yao, Y.; Tour, J. M.; Mayer, T. S.; Allara, D. L. *Nano Lett.* **2005**, *5*, 61-65.
33. Chen, X.; Jeon, Y.-M.; Jang, J.-W.; Qin, L.; Huo, F.; Wei, W.; Mirkin, C. A. *J. Am. Chem. Soc.* **2008**, *130*, 8166-8168.
34. Wang, G.; Kim, T.-W.; Lee, T. *J. Mater. Chem.* **2011**, *21*, 18117-18136.
35. Song, H.; Kim, Y.; Jang, Y. H.; Jeong, H.; Reed, M. A.; Lee, T. *Nature* **2009**, *462*, 1039-1043.
36. Gorman, C. B.; Carroll, R. L.; Fuierer, R. R. *Langmuir* **2001**, *17*, 6923-6930.
37. Wassel, R. A.; Credo, G. M.; Fuierer, R. R.; Feldheim, D. L.; Gorman, C. B. *J. Am. Chem. Soc.* **2004**, *126*, 295-300.
38. Cornil, J.; Karzazi, Y.; Brédas, J. L. *J. Am. Chem. Soc.* **2002**, *124*, 3516-3517.
39. Crivillers, N.; Paradinas, M.; Mas-Torrent, M.; Bromley, S. T.; Rovira, C.; Ocal, C.; Veciana, J. *Chem. Commun.* **2011**, *47*, 4664-4666.
40. Taylor, J.; Brandbyge, M.; Stokbro, K. *Phys. Rev. B* **2003**, *68*, 121101.
41. Chen, J.; Reed, M. A.; Rawlett, A. M.; Tour, J. M. *Science* **1999**, *286*, 1550-1552.
42. Galperin, M.; Ratner, M. A.; Nitzan, A. *Nano Lett.* **2005**, *5*, 125-130.
43. Yu, L. H.; Keane, Z. K.; Ciszek, J. W.; Cheng, L.; Stewart, M. P.; Tour, J. M.; Natelson, D. *Phys. Rev. Lett.* **2004**, *93*, 266802.
44. Reed, M. A. *Mater. Today* **2008**, *11*, 46-50.
45. Hipps, K. W.; Mazur, U. *J. Phys. Chem.* **1993**, *97*, 7803-7814.
46. Hipps, K. W. *Tunneling Spectroscopy of Organic Monolayers and Single Molecules*. In *Topics in Current Chemistry*, Metzger, R. M., Ed.; Springer-Verlag: Berlin, 2012; Vol. 313, pp 189-216.
47. Fock, J.; Sørensen, J. K.; Lortscher, E.; Vosch, T.; Martin, C. A.; Riel, H.; Kilsa, K.; Bjørnholm, T.; van der Zant, H. *Phys. Chem. Chem. Phys.* **2011**, *13*, 14325-14332.
48. Kouwenhoven, L.; Glazman, L. *Phys. World* **2001**, *14*, 33-38.
49. Scott, G. D.; Natelson, D. *ACS Nano* **2010**, *4*, 3560-3579.
50. Moth-Poulsen, K.; Bjørnholm, T. *Nat. Nanotechnol.* **2009**, *4*, 551-556.
51. Kubatkin, S.; Danilov, A.; Hjort, M.; Cornil, J.; Brédas, J.-L.; Stuhr-Hansen, N.; Hedegård, P.; Bjørnholm, T. *Nature* **2003**, *425*, 698-701.
52. Park, H.; Park, J.; Lim, A. K. L.; Anderson, E. H.; Alivisatos, A. P.; McEuen, P. L. *Nature* **2000**, *407*, 57-60.
53. Chae, D.-H.; Berry, J. F.; Jung, S.; Cotton, F. A.; Murillo, C. A.; Yao, Z. *Nano Lett.* **2006**, *6*, 165-168.
54. Jaklevic, R. C.; Lambe, J. *Phys. Rev. Lett.* **1966**, *17*, 1139-1140.
55. Kondo, J. *Prog. Theor. Phys.* **1964**, *32*, 37-49.
56. Yu, L. H.; Natelson, D. *Nano Lett.* **2004**, *4*, 79-83.
57. Liang, W.; Shores, M. P.; Bockrath, M.; Long, J. R.; Park, H. *Nature* **2002**, *417*, 725-729.
58. Park, J.; Pasupathy, A. N.; Goldsmith, J. I.; Chang, C.; Yaish, Y.; Petta, J. R.; Rinkoski, M.; Sethna, J. P.; Abruña, H. D.;

McEuen, P. L.; Ralph, D. C. *Nature* **2002**, *417*, 722-725.
59. Lee, J. T.; Chae, D.-H.; Yao, Z.; Sessler, J. L. *Chem. Commun.* **2012**, *48*, 4420-4422.
60. Houck, A. A.; Labaziewicz, J.; Chan, E. K.; Folk, J. A.; Chuang, I. L. *Nano Lett.* **2005**, *5*, 1685-1688.
61. Lansbergen, G. P.; Tettamanzi, G. C.; Verduijn, J.; Collaert, N.; Biesemans, S.; Blaauboer, M.; Rogge, S. *Nano Lett.* **2010**, *10*, 455-460.
62. Silbey, R. J.; Alberty, R. A.; Bawendi, M. G. *Physical Chemistry*; John Wiley & Sons Inc.: Hoboken, 2005; p 364.

